



Elevated Mixed Layers during Great Lake Lake-Effect Events: An Investigation and Case Study from OWLeS

STEVEN J. GREYBUSH,^a TODD D. SIKORA,^b GEORGE S. YOUNG,^a QUINLAN MULHERN,^a
RICHARD D. CLARK,^b AND MICHAEL L. JUREWICZ SR.^c

^a Department of Meteorology and Atmospheric Science, The Pennsylvania State University, University Park, Pennsylvania

^b Department of Earth Sciences, Millersville University, Millersville, Pennsylvania

^c NOAA/NWS/Weather Forecast Office, State College, Pennsylvania

(Manuscript received 20 December 2022, in final form 3 November 2023, accepted 6 November 2023)

ABSTRACT: Data from rawinsondes launched during intensive observation periods (IOPs) of the Ontario Winter Lake-Effect Systems (OWLeS) field project reveal that elevated mixed layers (EMLs) in the lower troposphere were relatively common near Lake Ontario during OWLeS lake-effect events. Conservatively, EMLs exist in 193 of the 290 OWLeS IOP soundings. The distribution of EML base pressure derived from the OWLeS IOP soundings reveals two classes of EML, one that has a relatively low-elevation base (900–750 hPa) and one that has a relatively high-elevation base (750–500 hPa). It is hypothesized that the former class of EML, which is the focus of this research, is, at times, the result of mesoscale processes related to individual Great Lakes. WRF reanalysis fields from a case study during the OWLeS field project provide evidence of two means by which low-elevation base EMLs can originate from the lake-effect boundary layer convection and associated mesoscale circulations. First, such EMLs can form within the upper-level outflow branches of mesoscale solenoidal circulations. Evacuated Great Lakes-modified convective boundary layer air aloft then lies above ambient air of a greater static stability, forming EMLs. Second, such EMLs can form in the absence of a mesoscale solenoidal circulation when Great Lake-modified convective boundary layers overrun ambient air of a greater density. The reanalysis fields show that EMLs and layers of reduced static stability tied to Great Lakes-modified convective boundary layers can extend downwind for hundreds of kilometers from their areas of formation. Operational implications and avenues for future research are discussed.

KEYWORDS: Snow; Numerical weather prediction/forecasting; Lake effects

1. Introduction

Great Lakes lake-effect snowstorms have garnered much attention from the research community because of their societal impacts, both positive (e.g., winter snow sports industry) and negative (e.g., highway transportation). For example, large-scale field measurements were collected as part of the Lake Ontario Winter Storms project in 1990 (Reinking et al. 1993) and the Lake-Induced Convection Experiment in 1997/98 (Kristovich et al. 2000). Complementary numerical modeling work includes Hjelmfelt (1990), Sousounis and Mann (2000), and Tripoli (2005). Collectively, those and related studies prompted several questions that are being addressed by the Ontario Winter Lake-Effect Systems (OWLeS) project. See Kristovich et al. (2017) for a thorough description of that field project and ongoing research.

OWLeS research is divided into several collaborative efforts, one of which is dubbed Surface and Atmospheric Influences on

Lake-Effect Convection (SAIL). The aim of OWLeS-SAIL is threefold. OWLeS-SAIL research is addressing 1) the upwind environmental influences on the overlake planetary boundary layer during lake-effect conditions, 2) the occasional persistence of lake-effect convection far downwind from the parent lake (Eipper et al. 2018, 2019), and 3) the varying structure of the planetary boundary layer as it advects over multiple bodies of water and intervening land under certain short-fetch conditions. A related thrust of OWLeS research concerns improving the understanding of the dynamics that drive the predictability of lake-effect snow through the use of numerical weather prediction, ensemble data assimilation, and reanalysis (e.g., Saslo and Greybush 2017; Seibert et al. 2022).

In the course of examining preliminary OWLeS field project data with other SAIL researchers, a particular rawinsonde sounding caught the interest of several of the authors of the present research. That sounding is replotted in Fig. 1. The data for that sounding were collected by collaborators from the State University of New York Oswego at 2013 UTC 6 January 2014 at Sodus Point, New York, during an intensive observation period (IOP). The lowest data point from the

Corresponding author: Steven J. Greybush, sjg213@psu.edu

DOI: 10.1175/MWR-D-22-0344.1

© 2023 American Meteorological Society. This published article is licensed under the terms of the default AMS reuse license. For information regarding reuse of this content and general copyright information, consult the AMS Copyright Policy (www.ametsoc.org/PUBSReuseLicenses).

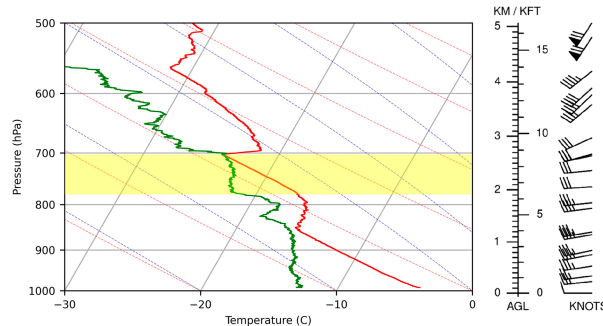


FIG. 1. Rawinsonde sounding based on data collected by collaborators at the State University of New York Oswego from 2013 UTC 6 Jan 2014 at Sodus Point during an OWLeS IOP. A well-defined EML exists in the 700–774-hPa layer, which has been highlighted in yellow.

original sounding is omitted from Fig. 1 because it was spurious (S. Steiger 2014, personal communication). Striking is the existence of a large lapse rate with a bottom-to-top increase in relative humidity in the 774–700-hPa layer. That layer is bounded above by what appears to be a subsidence inversion and below by a weaker statically stable layer above a surface-based mixed layer. Although shallow, the feature described above is reminiscent of a classic Midwestern elevated mixed layer (EML), such as that presented in Fig. 1 of Banacos and Ekster (2010). EMLs are one factor that impacts convection during severe weather setups in the Midwest region of the United States. There, EMLs are formed when continental tropical air from a higher elevation is advected over maritime tropical air, resulting in a capping inversion at the base of the layer (Carlson et al. 1983). Carlson and Ludlam (1968) show that the capping inversion associated with the EML can act to initially suppress convection on high-end severe weather days. Then, when this cap is erased (e.g., via entrainment and encroachment; Stull 1988), the EML's steep lapse rate enables a saturated and positively buoyant parcel at the base of the layer to rapidly accelerate upward, promoting strong vertical motion and deep moist convection.

The presence of EMLs in the context of lake-effect events is significant because, similar to Midwest EMLs, if any cap-like feature is overcome, the layer of near dry adiabatic lapse rates aloft may enable deeper and stronger lake-effect convection than would be present without the EML (assuming the EML overlays an area favorable for surface-based convection). This more vigorous convection could promote enhanced lake-effect snowfall downwind of the lake. On the other hand, if the cap is too strong to be overcome, the result would be a suppression of lake-effect convection. That logic begs the following research questions:

- 1) How common are lower-tropospheric (bases at pressures greater than or equal to 500 hPa) EMLs during Great Lakes lake-effect events?
- 2) What are the mesoscale processes by which EMLs can form in association with lake-effect events?
- 3) How far downwind can such EMLs extend from their parent lake?

Evidence of a mixed layer aloft in lake-effect settings is mentioned in Agee and Gilbert (1989). Chang and Braham (1991) and Schroeder et al. (2006; with a synoptically induced EML), indicated that the convective boundary layer can deepen rapidly after it penetrates into the EML. Lenschow (1973) also showed an EML over lake-effect convection (e.g., their Fig. 5), but the convection did not penetrate the EML. However, the authors are not aware of other studies that have addressed those three research questions. Thus, their objective herein is to begin to do so by leveraging the resources of the OWLeS project. The present research, which should be viewed as a pilot study, employs OWLeS IOP rawinsonde data to address question 1 (section 2) and reanalysis fields from a mesoscale model-based ensemble assimilation run for one case study to address questions 2 and 3 (section 3). A summary and recommendations for future work are provided in section 4.

2. OWLeS IOP rawinsonde soundings

The occurrence and nonoccurrence of EMLs during the 24 OWLeS IOPs were documented using data from the 290 OWLeS IOP rawinsonde soundings, which were launched by Hobart and William Smith Colleges, Millersville University, the State University of New York Oswego, the University of Illinois, and the University of Utah. The Illinois team launched upwind of Lake Ontario, along its northwest shore, whereas the other teams launched at a variety of sites downwind of Lakes Ontario and Erie, extending from the western Finger Lakes to the Tug Hill plateau in New York, with specific locations tailored to each IOP. Refer to Fig. 2 for the geography and topography of the Great Lakes region. Figure 2 also shows Weather Research and Forecasting (WRF) Model domains, which are discussed below.

The OWLeS rawinsonde data were downloaded from NCAR's Cooperative Distributed Interactive Atmospheric Catalog System (http://data.eol.ucar.edu/master_list/?project=OWLeS; Laird and Metz 2014; Clark 2014; Steiger 2014; Kristovich 2014; Steenburgh et al. 2014). The soundings include pressure, temperature, and dewpoint temperature at 1-s resolution, from which potential temperature was calculated. EMLs were objectively identified as follows. First, a 100-s moving window local linear regression fit (corresponding to a minimum layer thickness of approximately 0.5 km) was used to filter out noise in the soundings. Then any non-surface-based layer for which potential temperature increased by less than 2 K km^{-1} was categorized as an EML. The 2 K km^{-1} threshold is commonly employed to identify dry mixed layers (e.g., Garrett 1981; Nielsen-Gammon et al. 2008) and corresponds to a temperature lapse rate of around 8 K km^{-1} , which is consistent with previous studies looking at EMLs (Banacos and Ekster 2010; Cordeira et al. 2017; Ribeiro and Bosart 2018). Because the window was moved upward one observation point at a time, the window width does not impose an upper limit on the depth of identified EMLs. Results were spot-checked using corresponding plots of temperature, dewpoint temperature, and potential temperature versus pressure.

While the EML identification results are, of course, sensitive to the definition used, applying the above-mentioned methodology yields EMLs (with bases at pressures $\geq 500 \text{ hPa}$)

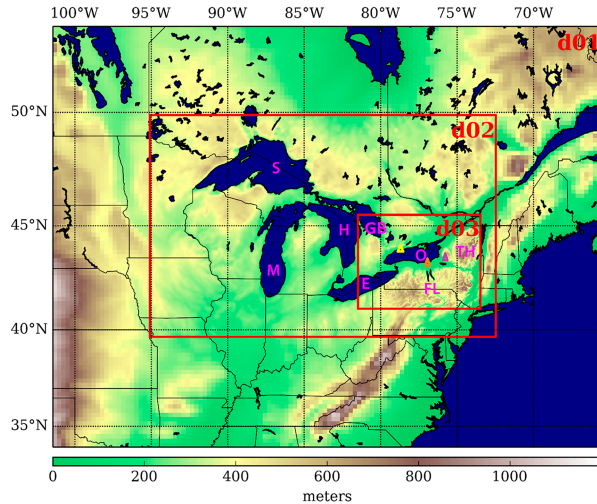


FIG. 2. Geography and topography (m above sea level) of the Great Lakes region (area roughly encompassed by box d02). Each Great Lake is identified by the first letter of its name (Superior, Michigan, Huron, Erie, and Ontario), GB denotes Georgian Bay, FL is placed just south of the Finger Lakes, and TH stands for Tug Hill. Domains d01, d02, and d03 are numerical weather prediction model domains used in this research. Triangles note the example location of soundings, including Sodus Point (orange; Fig. 1), Darlington (yellow), and Redfield (purple).

in 67% of the OWLeS IOP rawinsonde soundings examined. Thus, EMLs were a rather common phenomenon near Lake Ontario during the OWLeS field project. Figure 3a shows a histogram of EML base pressure derived from the OWLeS IOP soundings, binned every 25 hPa. There are two peaks in the distribution. One is the 850–825-hPa bin and the other is the 550–525-hPa bin, with a distinct minimum in the 750–725-hPa bin. Thus, Fig. 3a captures two classes of EML, one that has a relatively low-elevation base and one that has a relatively high-elevation base. Figure 3b shows the corresponding histogram of EML thickness, binned every 25 hPa. Here, no limit was placed on the pressure level of the top of an EML. The peak of the distribution is in the 75–100-hPa bin, and the majority have a thickness less than 150 hPa. These EMLs are shallower than those typically associated with severe convection (e.g., Ribeiro and Bosart 2018, where a minimum depth threshold of 150 hPa was applied). Shallower EMLs may still occur in severe convective environments but deeper layers are considered more important as they will have a stronger impact on updraft strength (hence the use of a minimum depth threshold in this and other studies). Note that the base of the EML highlighted in Fig. 1 fits with the low-elevation base class of EML from Fig. 3a, and that its thickness is very close to the peak in Fig. 3b.

Returning their attention to the two classes of EML evident in Fig. 3a, the authors speculate that high-elevation base EMLs largely arise due to synoptic-scale processes. For example, high-elevation base EMLs could lie above synoptic-scale frontal inversions. The authors' focus for the remainder of this research is on lower-tropospheric EMLs, which they hypothesize could, at

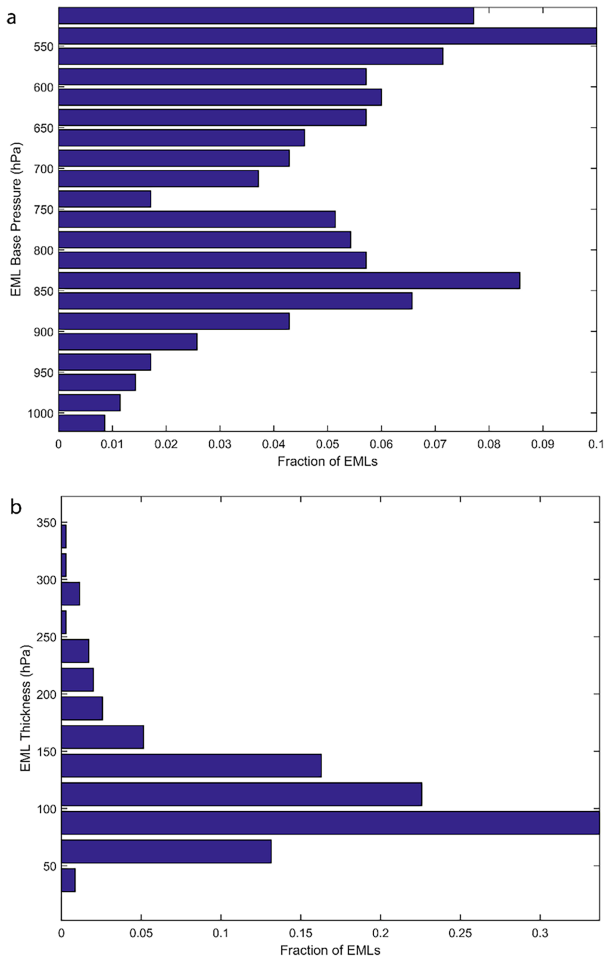


FIG. 3. Occurrence frequency histograms derived from the OWLeS IOP rawinsonde soundings of (a) EML base pressure and (b) EML thickness, using a threshold of 2 km^{-1} .

times, originate from the lake-effect boundary layer convection and associated mesoscale circulations. Because lake-effect convection is relatively shallow, it is unlikely to be augmented by EMLs located more than a few kilometers above the surface. EMLs are further explored in the following case study.

3. Case study with WRF Model-based ensemble assimilation run

a. Modeling and assimilation methodology

Further insights into the morphology of EMLs during lake-effect events were obtained from 21-member ensemble assimilation runs of version 3.7 of the WRF Model (Skamarock et al. 2008). The 21 members of the ensemble employed a one-way nested domain structure at 27-, 9-, and 3-km horizontal resolutions (see Fig. 2). Fields from the 9-km domain (shown in all figures unless otherwise indicated) are employed in the present research as they cover all five Great Lakes, while those from the 3-km domain are examined to explore the sensitivity of the results to horizontal grid spacing (see appendix). The outer domains

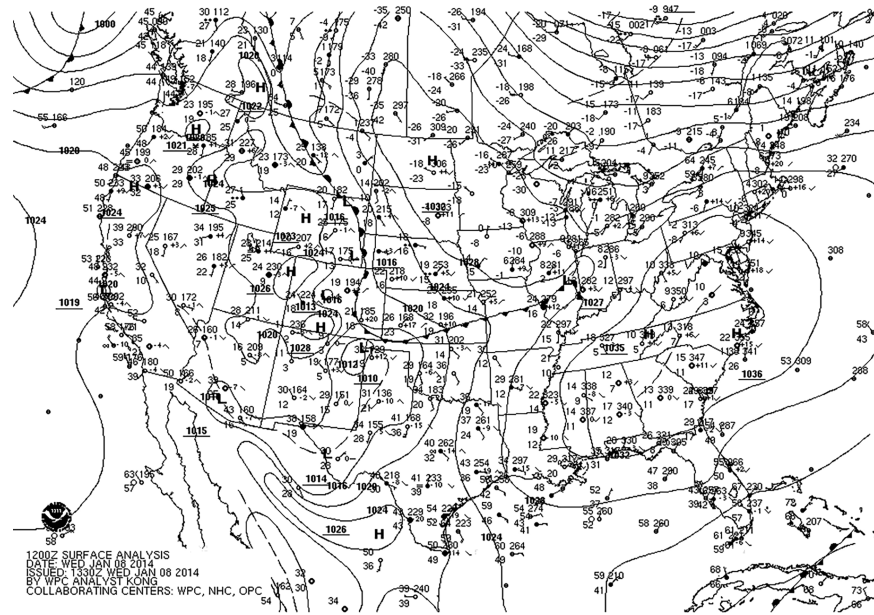


FIG. 4. WPC surface analysis (http://www.wpc.ncep.noaa.gov/archives/web_pages/sfc/sfc_archive.php), indicating mean sea level pressure, analyzed surface fronts, and station observations for 1200 UTC 8 Jan 2014.

used the Grell-3 convection scheme (Grell and Dévényi 2002), whereas the inner domain was convection allowing. The simulations used the two-moment Thompson microphysics scheme (Thompson et al. 2008), the Mellor–Yamada–Janjić boundary layer scheme (Janjić 1994), the ETA surface layer scheme (Janjić 1996, 2002), and the Noah land surface model (Chen and Dudhia 2001). We acknowledge that surface fluxes and lake-effect snowfall can be sensitive to the choice of turbulence scheme (Conrick et al. 2015; Minder et al. 2020). These runs employed 43 terrain-following levels in the vertical, with a model top of 50 hPa. For this study, data from the native WRF vertical levels were interpolated to pressure levels with a vertical resolution of 12.5 hPa from the bottom to 925 hPa, 25 hPa from 925 to 150 hPa, and 12.5 hPa from 150 hPa to the top.

Ensemble assimilation runs were created using the Pennsylvania State University ensemble Kalman filter (PSU-EnKF) data assimilation system (Zhang et al. 2006; Weng and Zhang 2012), which employs a serial ensemble Kalman filter (Whitaker and Hamill 2002). An important advantage of ensemble assimilation techniques is that they take advantage of flow-dependent forecast errors to characterize both the state (ensemble mean) and its uncertainty (ensemble spread). Boundary conditions for each of the 21 members of the ensemble came from the Global Ensemble Forecast System (GEFS). NCEP's real-time global sea surface temperature product was used to initialize lake surface temperatures and the National Ice Center's Interactive Multisensor Snow and Ice Mapping System was used for lake ice coverage. The PSU-EnKF system was cycled hourly, assimilating conventional observations (METAR, NWS rawinsonde, and ACARS aircraft data) on all three domains. OWLs field project data were not assimilated so that they could be used as independent validation of the resulting reanalysis fields for related research (Saslo and Greybush 2017).

The runs were initialized at 0600 UTC 6 January 2014, with data assimilation beginning 1200 UTC 6 January 2014 and extending through 0000 UTC 9 January 2014 allowing sufficient time for model spinup (e.g., Eure et al. 2023). Further details on the data assimilation and modeling, including sensitivity to ensemble configuration, predictability, and forecast evaluation with respect to field project observations, can be found in Saslo and Greybush (2017).

The resulting 9-km “best member” reanalysis fields are presented in section 3b. Using a best member maintains the advantage of employing an ensemble data assimilation technique to produce the analyses while concentrating on a single realization of the model fields that are expected to be closest to the actual state of the atmosphere. The methodology for determining the “best” ensemble member, or most representative member (MRM), is an adaptation of a method used in Lee et al. (2009) that is described in Eipper et al. (2019). First, a benchmark state is identified that the MRM is designed to represent. Although observations are clearly a valid option for this benchmark state, the authors choose instead to use the posterior ensemble mean. That mean is closely linked to observations through the PSU-EnKF data assimilation but has the advantage of a much higher spatial resolution and full dynamical fields. Horizontal components of the wind vector and temperature at 700 and 850 hPa are the variables used to assess closeness to the benchmark state, which we selected because of their importance to lake-effect convection. The closeness metric is the normalized mean absolute error (MAE), where the normalization accounts for the average MAE for each variable type across all ensemble members [see Eipper et al. (2019), their Eq. (A1)]. Examination of sensitivity to the choice of ensemble members has shown that EMLs are similar across ensemble members but may have subtle differences in lapse rate and thickness.

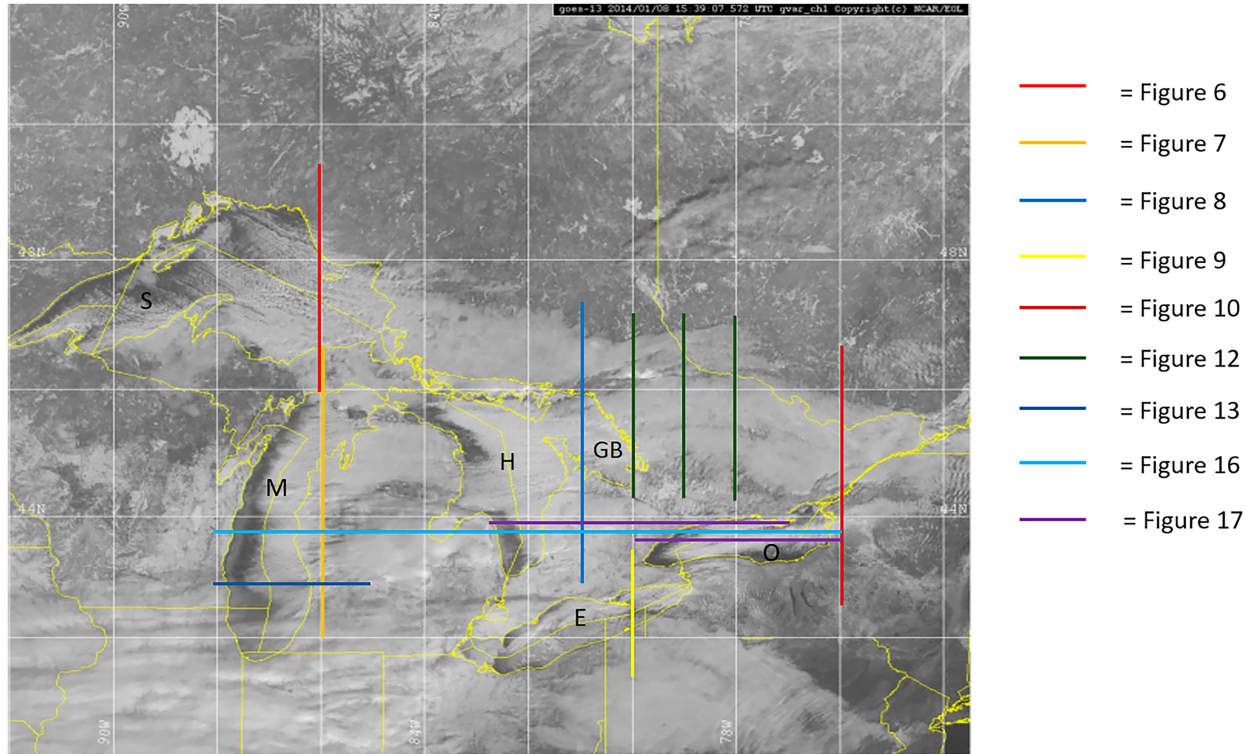


FIG. 5. GOES-13 visible satellite image from 1539 UTC 8 Jan 2014, downloaded from the OWLeS Field Catalog (<http://catalog.eol.ucar.edu/owles>). The five Great Lakes are identified by the first letter of their name, and Georgian Bay is labeled as GB. Locations of cross sections are denoted using colored lines.

b. Case study description

Keeping in mind the focus of the present research, we conducted ensemble assimilation runs for IOPs when OWLeS rawinsonde soundings revealed numerous EMLs. A single reanalysis time, 1200 UTC 8 January 2014, from the ensemble assimilation run initialized at 0600 UTC 6 January 2014 (with data assimilation proceeding from 1200 UTC 6 to 0000 UTC 9 January 2014), was chosen by the authors to serve as a primary case study for the present research. The authors chose that reanalysis time because, as will be shown below, mesoscale processes related to each Great Lake are collocated with EMLs in the reanalysis fields. Multiple examples of EMLs were present at this time, and therefore this single case study actually represents five subcase studies (one at each lake). In addition, plots from model output at a few other times are compared with rawinsonde data later in the paper, showing that the time selected for this case study is not unique in how it represents EMLs.

Figure 4 is a Weather Prediction Center (WPC) surface analysis from 1200 UTC 8 January 2014. At that time, a sea level pressure trough was over the Lower Peninsula of Michigan, with Arctic air throughout the Great Lakes region. Surface winds were generally westerly or southwesterly in the vicinity of the Great Lakes, which is along the major axis of Lakes Erie, Ontario, and Superior and the minor axis of Lake Michigan and Huron. The OWLeS field catalog revealed that lake surface temperatures over Lake Ontario were estimated to be

around 2°–6°C by the POES AVHRR SST product, although some 2-m temperatures downwind of the lake were reported as up to 16°C, with 2-m temperatures just upwind of the lake as cold as –15°C. A GOES-13 visible image from 1539 UTC 8 January 2014 (Fig. 5) reveals the cloud signatures of lake-effect convection over all five Great Lakes. Cloud streets are evident over Lake Superior (Young et al. 2002), whereas a long-lake-axis parallel (LLAP) band is found over Lake Ontario (Eipper et al. 2018). The authors chose to show the 1539 UTC visible satellite image because it was subjectively determined to be the first high-contrast visible image of the day. The colored lines within Fig. 5 show the location of reanalysis cross sections, discussed next.

c. Reanalysis cross sections

Figures 6–10 each contain three north–south vertical cross sections (a–c) of best-member reanalysis fields valid at 1200 UTC 8 January 2014. Panel a is $\partial\theta/\partial z$, where θ is potential temperature; panel b of each of those figures is the north–south component of the wind vector; and panel c is the vertical component of the wind vector. The cross-sectional longitudes are generally sequenced from west to east from Figs. 6 to 10, with each cross section focused on a particular lake; recall that Fig. 5 shows the locations of the cross sections relative to the Great Lakes. For each of those cross sections, the vertical axis is height above sea level and the horizontal axis is degrees latitude. The latitudinal extent of each cross section was chosen to highlight features of

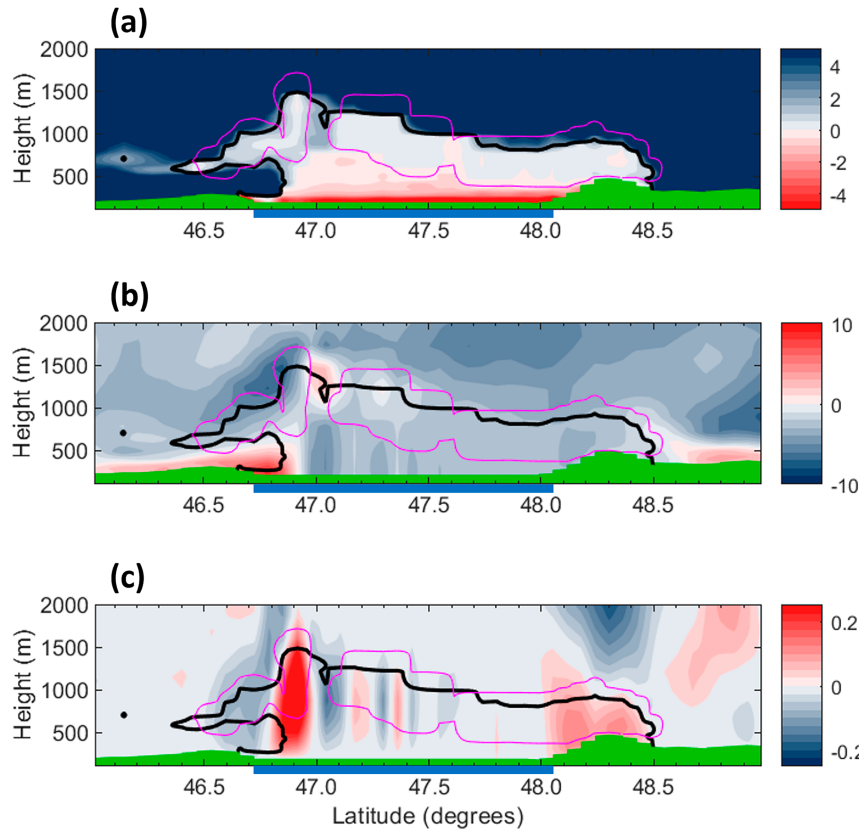


FIG. 6. North-south vertical cross sections along 86°W including Lake Superior (blue ribbon) of best-member reanalysis fields of (a) $\partial\theta/\partial z$ (K km^{-1}), (b) the north-south component of the wind vector (m s^{-1}), and (c) the vertical component of the wind vector (m s^{-1}). The thick black line indicates $\partial\theta/\partial z < 2 \text{ K km}^{-1}$ (our criterion for a mixed layer), and the magenta contour indicates cloudy regions (total cloud water content $> 0.01 \text{ g kg}^{-1}$). Each cross section is valid at 1200 UTC 8 Jan 2014. In this and subsequent cross-sectional figures, topography is shown in green, and, where applicable, the location of a Great Lake is denoted by a blue ribbon at the bottom of a cross section.

interest, and thus is not identical from one cross section to another.

Within panel a of Figs. 6–10, lake-modified convective boundary layers appear as surface-based layers of near dry adiabatic lapse rate ($\partial\theta/\partial z \approx 0$; whiter shading) over or downwind of the parent Great Lakes. For example, the convective boundary layer modified by Lake Superior extends from $\sim 46.8^\circ$ to $\sim 48.5^\circ\text{N}$ in Fig. 6a (and the northern part of Fig. 7a). In certain locations adjacent to those lake-modified convective boundary layers, EMLs exist: for example, between 500 and 1000 m from 46.3° to 46.8°N in Fig. 6a, 42.5° to 43.3°N in Fig. 7a, 45.5° to 45.9°N in Fig. 8a, 42.6° to 42.8°N in Fig. 9a, and 43.8° to 44.2°N in Fig. 10a. Elevated layers in which the static stability is notably reduced relative to the ambient environment, but that do not meet the strict 2 K km^{-1} threshold, extend over a wider region; herein, we refer to these as elevated reduced static stability layers (ERSSLs). These ERSSLs can be identified with a greater horizontal extent than the EMLs in a number of the plots; for example, from 45.6° to 46.8°N in Fig. 7a and 42.6° to 43.1°N in Fig. 9a.

It will be argued below that those highlighted EMLs are related to, via mesoscale processes, the convective boundary layers modified by Lakes Superior (Fig. 6a), Michigan (Fig. 7a), Huron (Fig. 8a), Erie (Fig. 9a), and Ontario (Fig. 10a). Caution, however, should be taken when assigning a specific portion of an EML to a certain Great Lake-modified convective boundary layer in panel a of Figs. 6–10, even if the two appear to be connected. This is especially true for the eastern cross sections because, as will be shown below, the signatures of such EMLs and ERSSLs can merge downwind.

The bases of the highlighted EMLs in panel a of Figs. 6–10 correspond to levels just below the peak of the EML distribution that is closest to the ground (Fig. 3a). Moreover, their center pressure levels are greater (i.e., at a lower elevation) than that of the EML highlighted in Fig. 1. It is possible that the vertical placement of EMLs tied to Great Lake-modified convective boundary layers can vary from case to case due to, among other reasons, synoptic-scale vertical advection of EMLs, the synoptic scale's influence on the base of the

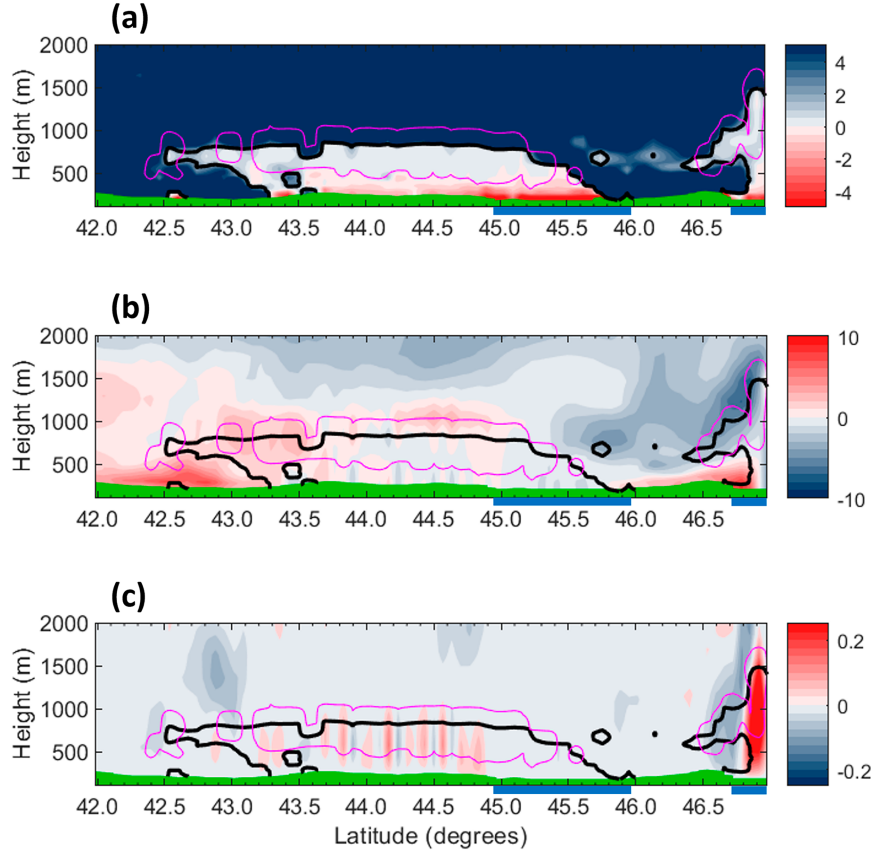


FIG. 7. As in Fig. 6, but along 86°W for Lake Michigan (larger blue ribbon). Note that the northmost section of blue ribbon is Lake Superior.

subsidence or frontal inversion that caps lake-effect convection (Nizioł 1987), and the depth of the ambient statically stable continental polar or Arctic air mass. Other factors may include the difference in temperature between the lake surface and the air being advected above it (larger differences promoting deeper convective overturning), and the speed and direction of ambient low-level wind (strong winds or reduced fetch can limit convective vigor).

d. Formation mechanisms

Having identified EMLs in panel a of Figs. 6–10, the interest now turns to their formation mechanisms. One plausible genesis mechanism is that some EMLs form in the diverging upper-level branches of mesoscale solenoidal circulations associated with Great Lake-modified convective boundary layers (Lavoie 1972; Hjelmfelt and Braham 1983; Laird et al. 2003; Steiger et al. 2013; Bergmaier et al. 2017). The reanalysis reveals that the lake-modified convective boundary layer of several of the Great Lakes yield mesoscale solenoidal circulations. In comparing panels b and c of Figs. 6 (Lake Superior), 8 (Lake Huron), 9 (Lake Erie), and 10 (Lake Ontario), one finds circulations reminiscent of long-lake-axis-parallel lake-effect convection (e.g., Bergmaier et al. 2017), including low-level inflow, updrafts, and upper-

level outflow. (The strong low-level southerlies near the southern portion of Fig. 8b precede the aforementioned sea level pressure trough.) The ascending branches of those circulations are located at approximately 46.8°, 45.4°, 42.4°, and 43.7°N, respectively (note that we focus on the dominant updrafts in each plot, rather than the periodic weaker updraft signals at other locations in the model domain). In contrast, Fig. 7 shows that a distinct mesoscale solenoidal circulation is not associated with the Lake Michigan-modified convective boundary layer, in either the horizontal or vertical velocity field.

The interlake variability described above is expected given the satellite image shown in Fig. 5. Note from the cloud signatures therein that the eastern portion of Lakes Superior, Lakes Erie and Ontario, and the northern portion of Lake Huron, are generally experiencing long-fetch conditions, which is optimal for the type of mesoscale secondary circulation described above. In comparing the simulations to satellite (Fig. 5), some lakes are dominated by a single LLAP band (Lakes Erie and Ontario), whereas others have multiple lines of convection (Lakes Superior and Huron). Even when multiple lines of convection are present, so are solenoidal circulations (e.g., Young et al. 2002). Meanwhile Lake Michigan and the southern extent

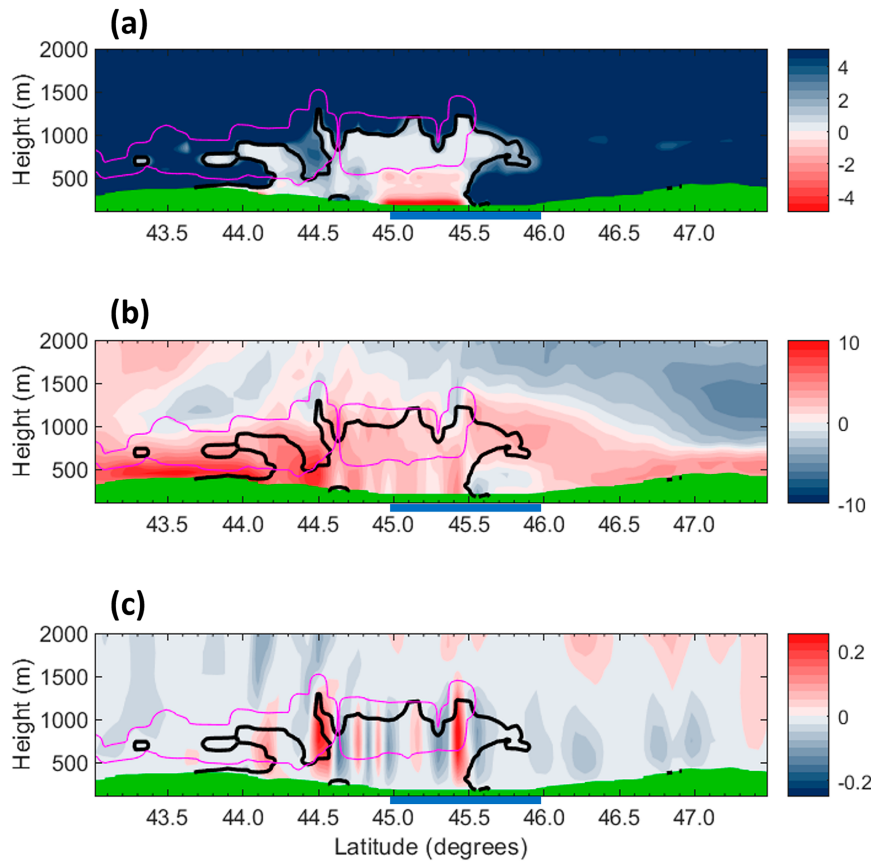


FIG. 8. As in Fig. 6, but along 81°W for Lake Huron/Georgian Bay. Note that the blue ribbon denotes the intersection with Georgian Bay.

of Lake Huron are experiencing short-fetch conditions, which is suboptimal (Kristovich et al. 2017) and explains the lack of solenoidal circulation in Fig. 7.

Mesoscale solenoidal circulations allow evacuated lake-modified convective boundary layers aloft to lie above ambient air of a greater static stability, thus giving rise to EMLs. Figure 11a depicts a schematic diagram of this formation mechanism involving the outflow at the top of mesoscale solenoidal circulations, which develop due to the heating of air as it passes over the lake surface and the pressure gradients that develop in response to this heating. At the lake surface, parcels of air will begin to rise and cool at the dry adiabatic lapse rate in an absolutely unstable environment for a brief time before the environmental lapse rate also becomes dry adiabatic. The potential temperature of the air parcels will remain the same (it will be that of the potential temperature at the lake surface) until they reach the lifting condensation level (LCL). It is here that an air parcel's potential temperature may increase slightly, but the temperature will continue to cool at the saturated adiabatic rate, which is close to dry adiabatic given such a cold environment. With increasing height, the potential temperature surrounding the parcel has remained very close to constant, but it begins to increase rapidly in the presence of a subsidence or

frontal inversion at the top of the boundary layer. When the surface-based virtual parcel potential temperature equals that of the environment, it can no longer accelerate upward and is forced outward in the form of outflow. These parcels of well-mixed lake-modified air displace air of greater static stability at the sides of the updraft, leaving pockets of more statically stable (denser) air under them. The layer of well-mixed parcels is then wedged between the statically stable air forced under the outflow and the statically stable air associated with the frontal inversion above it, resulting in an EML.

Evidence of this formation mechanism can be seen within Figs. 6 and 8–10. Because asymmetries exist between the upper-level outflow branches of the circulations, EMLs are favored to the south in Fig. 6, and to the north in Figs. 8–10. The reason for those asymmetries is beyond the scope of the present research but is certainly intriguing. Indeed, cases of symmetric (mushroom cap-like) EMLs have been documented that fit the mesoscale solenoidal circulation genesis paradigm (Sikora et al. 2015). One possibility, in keeping with mesoscale solenoidal circulation dynamics, is corresponding asymmetry in baroclinicity, with a circulation being strongest on the lake side adjacent to the coldest overland air mass. But other possibilities exist, such as the

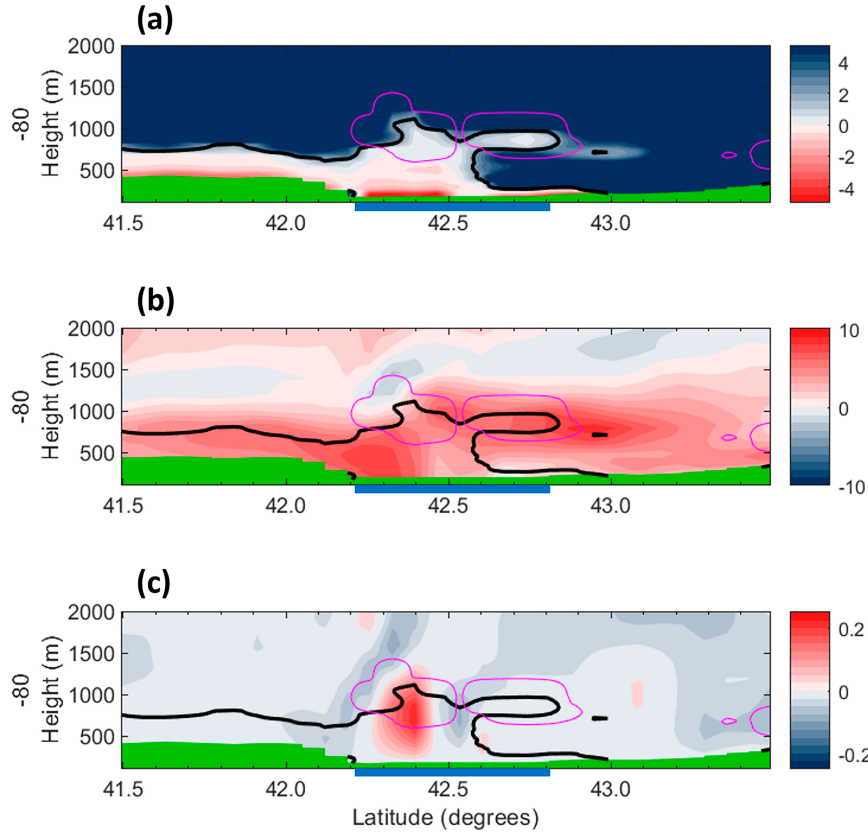


FIG. 9. As in Fig. 6, but along 80°W for Lake Erie.

influence of mesoscale frontal circulations, as described in Steenburgh and Campbell (2017) and Bergmaier et al. (2017). Advection of EMLs by the synoptic-scale wind is another possibility. This topic is left to future research.

As solenoidally driven EMLs extend downwind, it is possible for the low-level inflow of ambient air from opposite sides of the mesoscale updraft to meet, cutting off surface-based convection. When this occurs, the entire Great Lakes-modified convective boundary layer becomes elevated. In keeping with the mushroom analogy, the EML no longer has an associated stem to the surface. For the case study presented herein, examples of this process exist for the Lake Superior EML and Lake Huron EML. In Fig. 8 (81°W), convergence in the meridional wind is evident with a robust mixed layer and EML. Figure 12 shows several north–south vertical cross sections of $\partial\theta/\partial z$ east of Lake Huron, moving farther downstream (east) from the lake in successive panels. In Fig. 12a (along 80°W) we see the convective boundary layer and an associated EML immediately downwind of Georgian Bay in the south, which connects to an ERSSL that extends farther north. Based on the cloud features in the satellite imagery (Fig. 5) this is likely associated with convection over Lake Huron, and possibly Lake Superior, farther upstream. In Fig. 12b (along 79°W) the mixed layer is no longer connected to the ground, with a more limited EML but noticeable ERSSL aloft. Finally, by Fig. 12c (along 78°W),

only a patchy ERSSL aloft remains. The elongation of weak static stability at ~1000 m is a consequence of the Lake Superior and the Lake Huron mixed layers (the tracking of individual EMLs is discussed below) becoming separated from the surface.

It is also possible that EMLs tied to a Great Lake-modified convective boundary layer can form in the absence of a mesoscale solenoidal circulation. For example, it is plausible that EMLs can form downwind of a parent Great Lake when the upper part of that lake's modified convective boundary layer gets advected downstream and overruns an ambient statically stable continental polar or Arctic air mass of greater density. This mechanism is the consequence of differential advection and is similar to the process in which traditional EMLs in the Great Plains are formed (albeit the latter is over much larger spatial distances). The best example of this mechanism for the case study presented herein is the Lake Michigan EML, due to the lack of a strong mesoscale solenoidal circulation associated with the Lake Michigan-modified convective boundary layer (there is evidence for a weak circulation at 86°W in Fig. 13b). The reanalysis reveals a southerly near-surface jetlike feature along and just east of the sea level pressure trough over the lower peninsula of Michigan (this feature was alluded to above, in reference to Fig. 8b). The Lake Michigan-modified convective boundary layer lofted

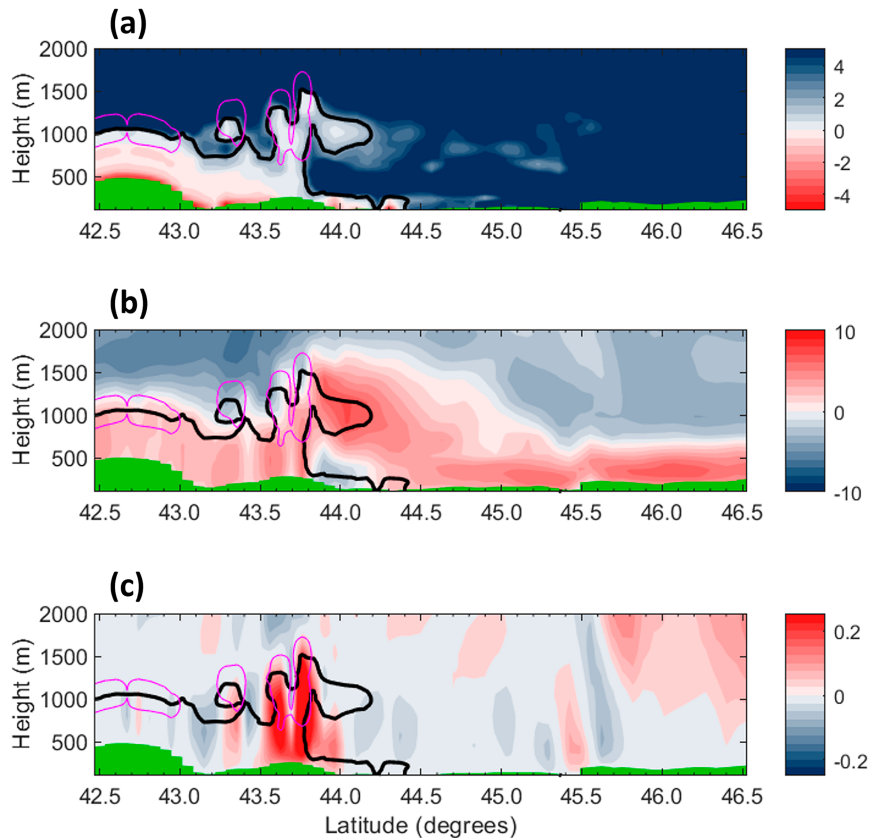


FIG. 10. As in Fig. 6, but along 76°W for Lake Ontario. Note that this cross section is downwind of Lake Ontario and therefore does not intercept the lake.

over that feature, thus forming an EML (cf. Figs. 7a,b). To further elucidate, Fig. 13 shows east–west cross sections of $d\theta/dz$, zonal wind u , and meridional wind v across Lake Michigan along 42.8°N. The EML of interest extends from

86.2° to 85.7°W, and between 600 and 800 m in altitude, with an ERSSL extending to 85.1°W. Evidence of the aforementioned overrunning exists to the east of the lake shore.

Figure 14 shows a schematic diagram illustrating the formation mechanism of EMLs involving the lofting of a well-mixed, lake-modified convective boundary layer over a more statically stable airmass of greater density. The temperature difference between the relatively warm lake surface and advected cold air (which often arrives after the passage of a cold front) above the surface leads to conditionally unstable or absolutely unstable conditions over the Great Lakes. As a result, the boundary layer above the lake becomes very well mixed and potential temperature (equivalent potential temperature if saturation occurs) is conserved with height throughout the layer. In the diagram, the arrows on the left represent the component of the synoptic scale wind parallel to the fetch of the lake. The longer the arrow, the greater the wind speed. An increasing wind speed with height, combined with the growth of the boundary layer across the fetch of the lake, would result in an upward sloping lake-modified CBL top. The wind then acts to advect the lake-modified CBL over the denser, statically stable air established over land and under the subsidence or frontal inversion present. The result is a layer of well-mixed lake modified CBL air resting on top of a more statically stable air mass, or an EML. The denser boundary layer air in this diagram

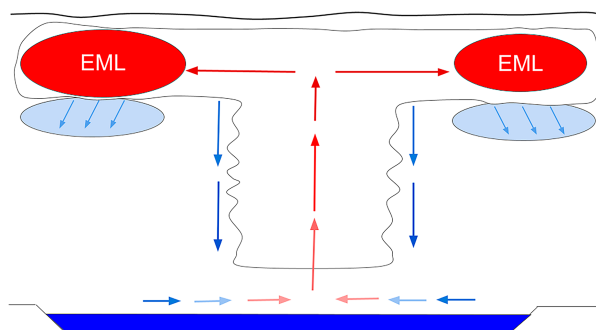


FIG. 11. Schematic diagram of a lake-effect mesoscale solenoidal circulation and its outflow resulting in EMLs. In the center, lake-modified air rises and condenses over relatively warm lake water. Aloft, modified CBL air in outflow displaces colder air from the surroundings. Slanted blue arrows display denser, statically stable air being forced under the elevated layer of lake-modified air. Blue downward-pointing arrows represent the cool downdraft associated with the solenoidal circulation.

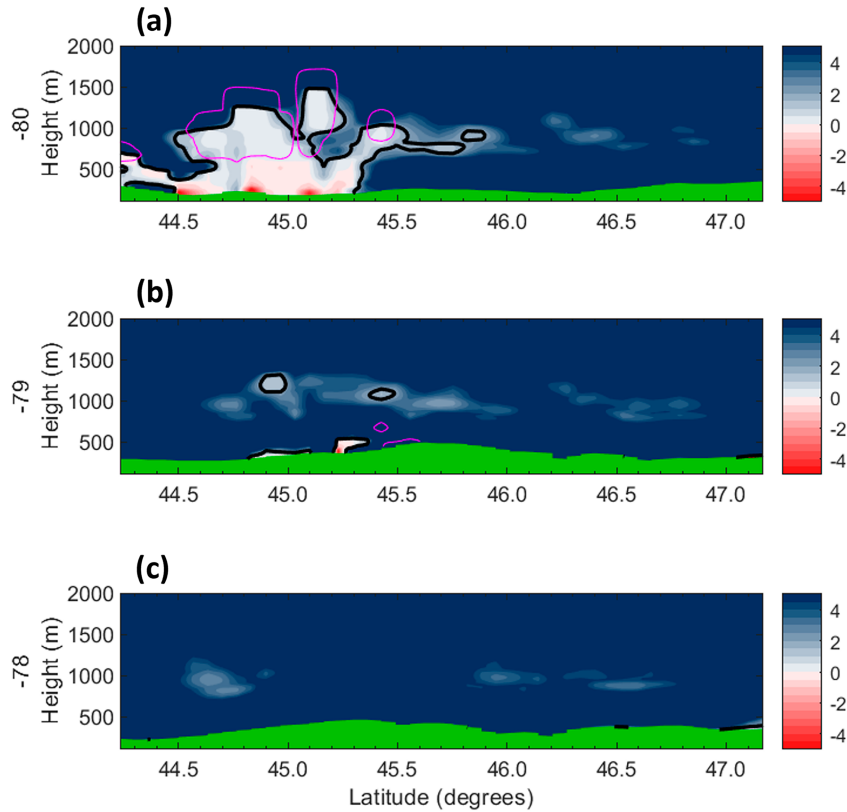


FIG. 12. North-south vertical cross sections along (a) 80°W , (b) 79°W , and (c) 78°W downwind of Lake Huron in eastern Ontario/southwestern Quebec, of best-member reanalysis fields of (a) $\partial\theta/\partial z$ (K km^{-1}). Each cross section is valid at 1200 UTC 8 Jan 2014.

essentially comes from two sources: colder Arctic air that has reached the downwind location unmodified by the lakes, or air that has been less dramatically modified by an upstream lake. Following the passage of a cold front, it is possible that surface winds were out of the northwest, ushering in cold air over both the Great Lakes and land surrounding the lakes. At the time of this study, none of the western lakes (Superior, Huron, or Michigan) were completely frozen, so any cold air advected over the warmer lakes would begin to heat up after infiltrating the lakes' CBLs before moving over land. However, this air would still be much cooler, statically stable, and more dense than air associated with the CBLs of the lakes themselves. If the cold air advected from the northwest did not come into contact with the lakes' CBLs and remained over land, then there would be a constant supply of even denser air. There may also be instances where relatively cold air is advected from south of the lakes. Even with a southerly wind and warm air advection, the air being brought north may still be much cooler than that associated with lake-modified CBLs. This would especially be the case if a surface high were located over the southeastern United States and much of the region was dominated by a continental polar airmass.

e. Plan view analysis and lake interactions

Figure 15 shows a plan view of the base height of EMLs and ERSSLs from the reanalysis. For Fig. 15a, an EML was defined

as any non-surface-based layer with a thickness of at least 25 hPa and with a $\partial\theta/\partial z$ less than 2 K km^{-1} . For comparison, in Fig. 15b, an ERSSL was defined as any non-surface-based layer with a thickness of at least 25 hPa and with a $\partial\theta/\partial z$ less than 5 K km^{-1} . The layer thickness threshold of 25 hPa is the minimum thickness resolved through the bulk of the troposphere in the pressure-interpolated reanalysis. For those locations where multiple qualifying layers are present in the reanalysis, only the base with the lowest elevation is plotted. Figure 15c shows the locations that have an EML or ERSSL with a base height below 1500 m.

EMLs tied to lake-modified convective boundary layers with base heights between 500 and 1500 m (Fig. 15a, depicted as shades of gold in the figure, and Fig. 15c, depicted in purple) extend downwind of each of the lakes, with EMLs extending in some areas from Lakes Michigan to Huron, Superior to Huron, and Huron and Erie to Ontario. These areas are generally found over land in between and downwind of the lakes, because over the lakes the mixed layers are connected to the surface and therefore excluded by our criteria used to identify EMLs; the layers are then advected downwind of the lakes. Certain gaps and breaks in the bases (e.g., at the southern tip of Lake Huron) reflect the penetration of EMLs by convective boundary layers (discussed in more detail below). When considering not just

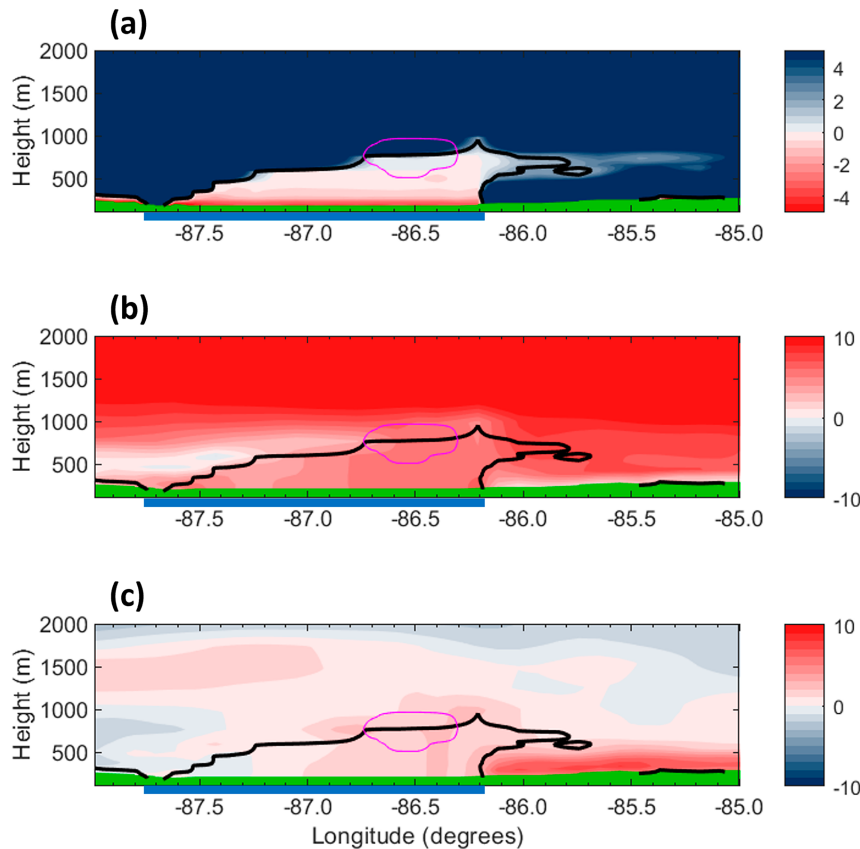


FIG. 13. East–west vertical cross sections along 42.8°N, including Lake Michigan, of best-member reanalysis fields of (a) $\partial\theta/\partial z$ (K km^{-1}), (b) the east–west component of the wind vector (m s^{-1}), and (c) the north–south component of the wind vector. Each cross section is valid at 1200 UTC 8 Jan 2014.

EMLs but ERSSLs (Figs. 15b,c), the inland extent and interaction with other lakes is increased, with a broad, interconnected region connecting Lake Superior with Huron and Ontario, and Michigan with Huron, Erie, and Ontario. EMLs may weaken into ERSSLs as they are advected downwind through entrainment and mixing with unmodified ambient air.

The bases of two relatively large-scale ERSSLs can be seen within Fig. 15b. The base of one of those ERSSLs slopes upward from the southwest corner of the figure toward the northeast, until obscured by other ERSSLs. That sloping base spans most of the histogram seen within Fig. 3a. It appears to be associated with the top of a sloping synoptic-scale frontal inversion. Indeed, warm frontogenesis was analyzed by WPC to the south of the Great Lakes between 1200 and 1800 UTC on 8 January 2014 (http://www.wpc.ncep.noaa.gov/archives/web_pages/sfc/sfc_archive.php). The large-scale ERSSL, with a base at approximately 2000 m, that blankets the northeast part of Fig. 15b most likely reflects the intersection of the denser, statically stable synoptic scale Arctic air mass (see surface high pressures located on the surface analysis in Fig. 2) and less statically stable air aloft. Additional evidence can be found in Fig. 10, where there is a pronounced decrease in

static stability (at the intersection of the air masses) above 500 m between 44° and 46°N. Thus, the reanalysis shows that ERSSLs are not exclusively the result of mesoscale processes, with higher-altitude ERSSLs largely arising from synoptic-scale processes.

On some occasions, a convective boundary layer can encroach upon an EML or ERSSL, and the presence of these layers aloft may contribute to more vigorous and deeper convection over a downstream lake due to the associated reduction in static stability. Figure 16, an east–west vertical cross section of $\partial\theta/\partial z$ along 43.75°N presents an example of such. The EML that begins near 85°W is tied to the Lake Michigan-modified convective boundary layer as described above. That EML (then ERSSL) extends eastward toward the southern tip of Lake Huron, and the reduced static stability within the layer may enhance convection over the downstream lake. There, the Lake Huron-modified convective boundary layer penetrates the Lake Michigan ERSSL (at $\sim 82^{\circ}\text{W}$). The location of that penetration (Fig. 16b) matches nicely with the data presented in Fig. 15 and also seems to be manifested in the GOES-13 visible image found in Fig. 5, where the scene goes from clear (parcels not reaching their LCL) to cloudy (parcels reaching their LCL). The Lake

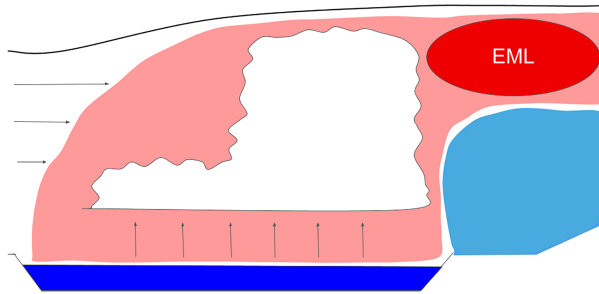


FIG. 14. Schematic diagram of a lake-effect EML, demonstrating the lofting of a lake-modified CBL resulting in an EML. A lake-modified CBL is advected over denser, statically stable air, forming an EML.

Huron EML then proceeds downwind to make contact with the robust convection over Lake Ontario. That ERSSLs interconnect between the lakes on two different dates (Figs. 16a,b) shows that these are not isolated or rare occurrences.

f. Comparison of model cross sections and OWLeS soundings

This section links together two aspects of the paper: the OWLeS soundings that motivated the exploration of EMLs, and corresponding model cross sections. The 0815 UTC 7 January 2014 sounding from Darlington, Ontario, Canada (on the northwest shore of Lake Ontario), is shown in Fig. 17a. Here, a well-mixed layer extends from the surface to around 900 m, with a statically stable layer atop it through 1500 m, followed by a deep layer of $\partial\theta/\partial z$ values less than 2 K km^{-1} extending to above 4000 m. These layers are also present in the WRF thermodynamic analysis (Fig. 17c). While the lower mixed layer originates from Lake Ontario and is bounded above by the intervening statically stable layer, the upper ERSSL connects all the way to Lake Huron upstream. The 1115 UTC 7 January 2014 sounding from the North Redfield, New York, site [~ 20 mi (32 km) east of Lake Ontario shoreline] displayed relatively interesting features (Fig. 17b). The θ profile exhibited a 100-m-thick absolutely unstable layer extending from the surface before giving way to a well-mixed layer extending up to 800 m above sea level. Although Redfield is not located along the lakeshore, its unstable surface layer was the result of strong surface westerlies driving the lake-modified air inland and up the windward side of Tug Hill Plateau. A relatively shallow statically stable layer is present from 800 to 1000 m before another deep layer of well-mixed air becomes present from 1000 to 2700 m. It is this deep layer of $\partial\theta/\partial z$ values less than 2 K km^{-1} that is striking. WRF thermodynamic analysis at 1200 UTC (Fig. 17d), shortly after the Redfield launch, exhibits mixed, lake-modified air extending from the ground to 800–1000 m altitude capped by a statically stable layer that continues east of Lake Ontario. Above that, an EML with thickness greater than 1500 m extends from over the lake and downstream toward the east; it is this new mixed layer that is found in the Redfield sounding resting above the shallow statically stable layer.

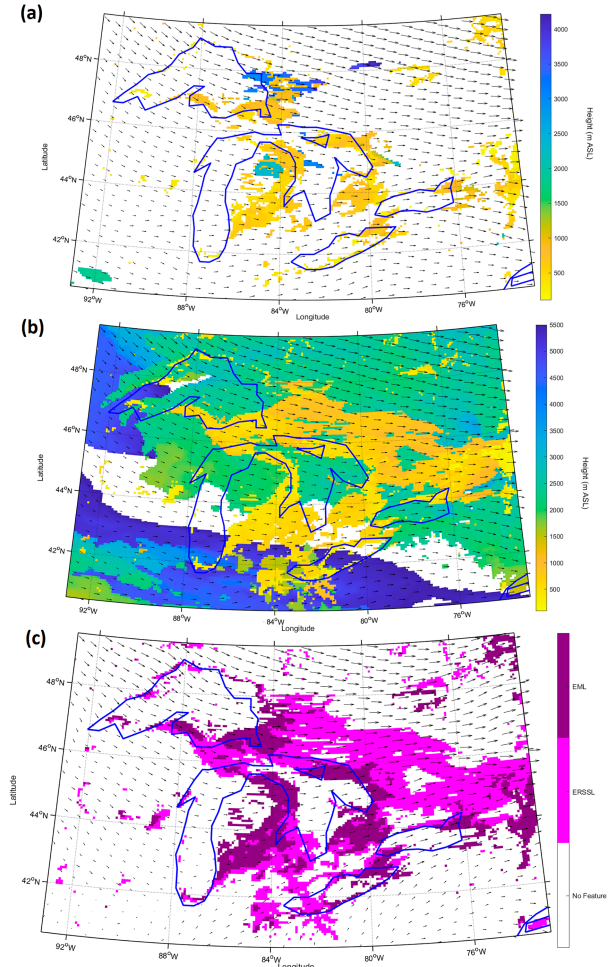


FIG. 15. Plan view of (a) EML and (b) ERSSL base height (m; shaded) and 1500-m winds (m s^{-1} ; arrows) for the best-member reanalysis valid at 1200 UTC 8 Jan 2014, and (c) an image mask (shading) denoting an EML or ERSSL with base heights below 1500 m, with 750-m winds (m s^{-1} ; arrows). For those locations where multiple layers are present in the reanalysis, only the base with the lowest elevation is plotted. For this figure, an EML was defined as any non-surface-based layer with a thickness of at least 25 hPa and with a $\partial\theta/\partial z$ less than 2 K km^{-1} , whereas an ERSSL was defined similarly except using a threshold of 5 K km^{-1} . White areas indicate that no layer is present that meets the criteria.

4. Summary

Lower-tropospheric EMLs were detected in 67% of rawinsonde soundings collected in support of the Ontario Winter Lake-Effect Systems field project (Kristovich et al. 2017). Further analysis of that rawinsonde data reveals two classes of EML, one that has a relatively high-elevation base (distribution peak of 550–525 hPa) and one that has a relatively low-elevation base (distribution peak of 850–825 hPa). It is hypothesized that some EMLs of the low-elevation base class originate from the lake-effect boundary layer convection and associated mesoscale circulations.

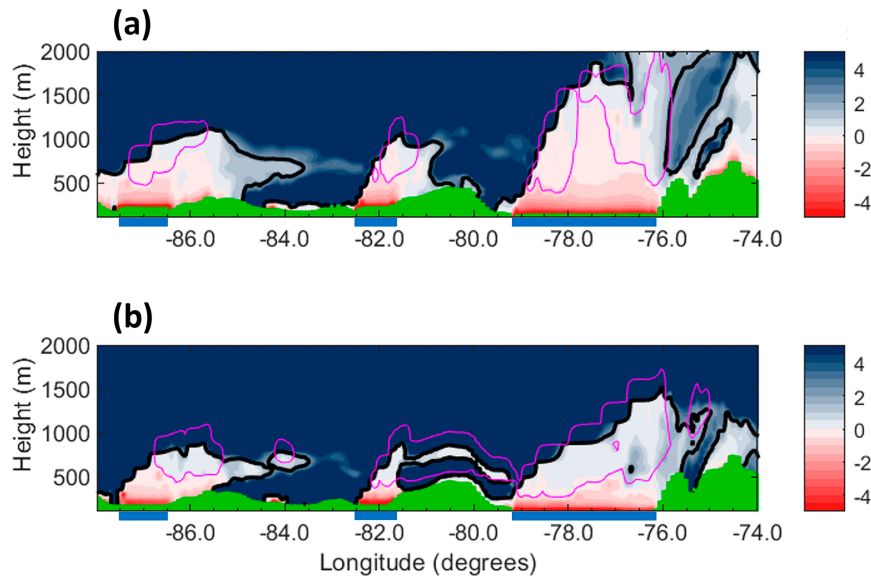


FIG. 16. East–west vertical cross section along 43.75°N , extending over Lakes Michigan, Huron, and Ontario, of the best-member reanalysis field of $\partial\theta/\partial z$ (K km^{-1}). The cross section is valid at (a) 1200 UTC 7 and (b) 1200 UTC 8 Jan 2014.

Indeed, results from WRF model-based ensemble assimilation run reanalysis fields provide evidence that such EMLs can form downwind of a parent Great Lake when that lake's modified convective boundary layer overruns an ambient denser, statically stable continental polar or Arctic air mass. Results also provide evidence that such EMLs can form within the upper-level outflow branches of mesoscale solenoidal circulations. The upper-level outflow branches are occupied by evacuated Great Lake-modified convective boundary layer air, beneath which is found ambient air of a greater static stability. In addition, results show that EMLs and Elevated Reduced Static Stability Layers (ERSSLs) tied to Great Lake-modified convective boundary layers can extend for hundreds of kilometers downwind of their associated lake. Thus, there is considerable opportunity for those EMLs and ERSSLs to interact with convective boundary layers over which they are found. For example, for the reanalysis presented herein, the Lake Huron-modified convective boundary layer penetrates the Lake Michigan ERSSL. In contrast, the convective boundary layer modified by Lake Ontario and overlying statically stable layer is topped by Lake Ontario's own ERSSL, indicating that both outcomes are possible.

Each of the above-described effects on downwind convective boundary layers could have potentially important consequences with regard to the character, positioning, and intensity of associated lake-effect precipitation bands. As such, particularly in an operational forecast setting, investigation and diagnoses of EMLs tied to Great Lake-modified convective boundary layers could provide valuable insight into the anticipated sensible weather impacts.

Building upon this and other studies, a detailed study about how such EMLs and ERSSLs influence downwind lake-effect precipitation bands would be an excellent opportunity for

future research. Such a study could leverage the OWLeS dataset with idealized model simulations (e.g., model runs with and without certain Great Lakes present). Other avenues for future research include the construction of a broader EML climatology for the Great Lakes region, as well as further investigation of EML genesis mechanisms, based on that climatology, to reveal the robustness of the preliminary results presented herein. Such future research could continue to employ the OWLeS dataset. But future research could also rely on the operational rawinsonde network as well as data from the New York State Mesonet (<http://www.nysmesonet.org>), which has been enhanced to include profiling data at various surface stations, including in the vicinity of Lakes Erie and Ontario.

Acknowledgments. The authors thank Daniel Eipper for supplying ensemble best-member information; Seth Saslo for his assistance in running simulations; Fuqing Zhang for his insights on modeling and data assimilation; the OWLeS principal investigators for their field collaborations; the NCAR archive managers for facilitating access to the OWLeS observations; the rawinsonde sounding teams from Hobart and William Smith Colleges, Millersville University, the State University of New York Oswego, the University of Illinois, and the University of Utah for professionalism under adverse meteorological conditions; and the anonymous reviewers and the editors for their thorough critique of the paper. Authors Sikora and Clark thank the staff of Finger Lakes Technical and Career Center for hosting the Millersville University OWLeS base of operations. Author Greybush thanks the Pennsylvania State University Institute for Computational and Data Sciences for providing the computing resources used to create the reanalyses. Authors Sikora, Young, and Clark were funded under OWLeS

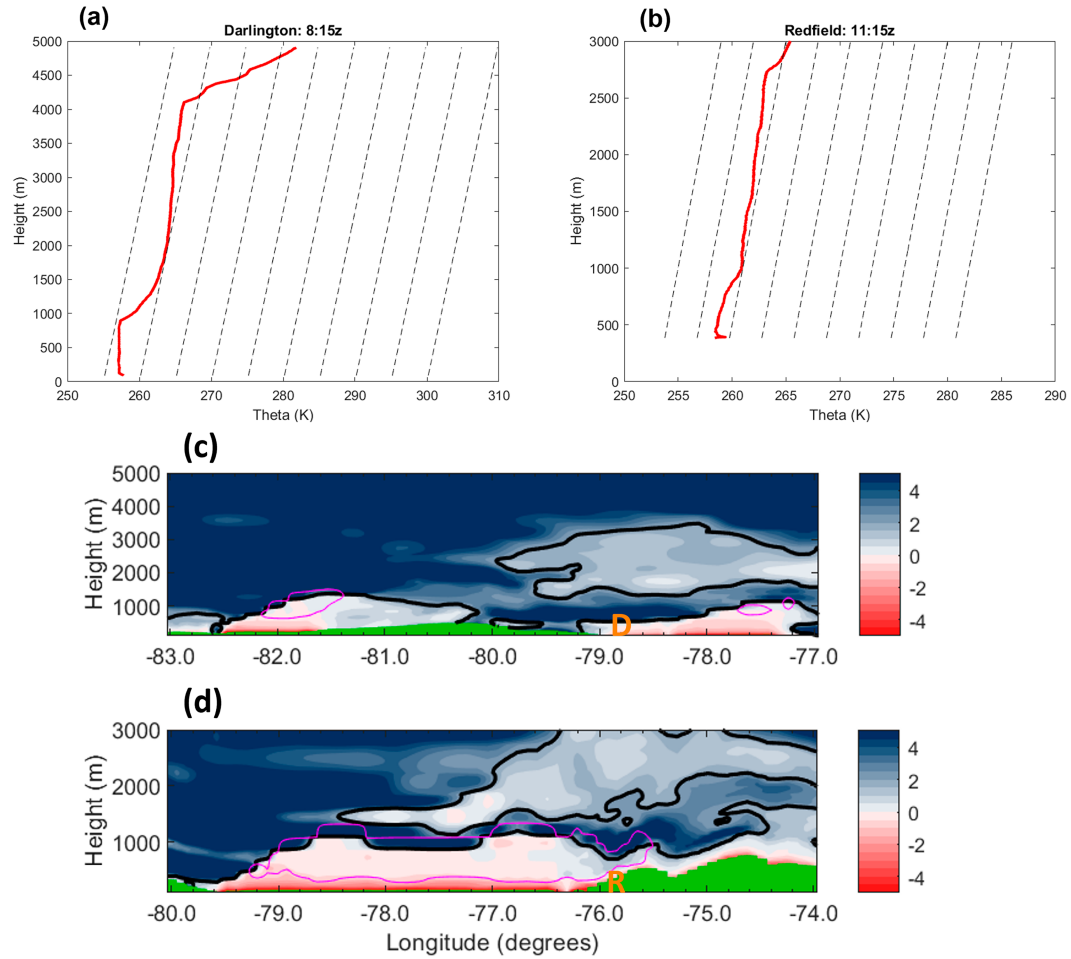


FIG. 17. OWLeS soundings for (a) Darlington at 0815 UTC 7 Jan 2014 and (b) Redfield at 1115 UTC 7 Jan 2014 in terms of potential temperature. Dashed lines indicate the threshold lapse rate of 2 K km^{-1} . Also shown are east–west vertical cross sections along the latitude of (c) Darlington and (d) Redfield of the best-member reanalysis field of $\partial\theta/\partial z$ (K km^{-1}). The locations of Redfield (R) and Darlington (D) are indicated on the corresponding cross section.

by National Science Foundation Grants AGS 12 59020 (Millersville University) and AGS 12 59011 (The Pennsylvania State University). Authors Greybush, Mulhern, and Young were funded by National Science Foundation Grant AGS 17 45243.

Data availability statement. OWLeS soundings can be downloaded from NCAR’s Cooperative Distributed Interactive Atmospheric Catalog System (http://data.eol.ucar.edu/master_list/?project=OWLeS) and are provided through the courtesy of Hobart and William Smith Colleges (Laird and Metz 2014), Millersville University (Clark 2014), the State University of New York Oswego (Steiger 2014), the University of Illinois (Kristovich 2014), and the University of Utah (Steenburgh et al. 2014). The WRF Model is a publicly available community model. Conventional observations used for data assimilation are available from NCEP. Analysis and simulation fields can be downloaded from the Pennsylvania State University Data Commons (Greybush and Young 2023).

APPENDIX

Sensitivity of Results to Model Horizontal Grid Spacing

We compared two cross sections (Fig. A1) spanning Lake Ontario, one at 3-km grid spacing (convection permitting) and one at 9-km grid spacing (using a convection parameterization). In the cross section, one can see the finer-scale terrain at 3 km while both resolutions represent the Tug Hill Plateau and Adirondacks. Overall, the two figures show similarities in large-scale features: an unstable layer of air (with negative lapse rates; red shading) located over Lake Ontario and a near-neutral layer (white and light blue) above it, which extends downstream over the Tug Hill plateau, as well as a narrow elevated layer upstream of the lake. Although there are some differences in the details (e.g., the linear extent of the upstream EML/ERSSL and the precise lapse rate in the downstream EML/ERSSL), this comparison gives us confidence that the 9-km simulations can adequately describe EMLs/ERSSLs in the Great Lakes region. We also recognize that, because of limitations in vertical resolution,

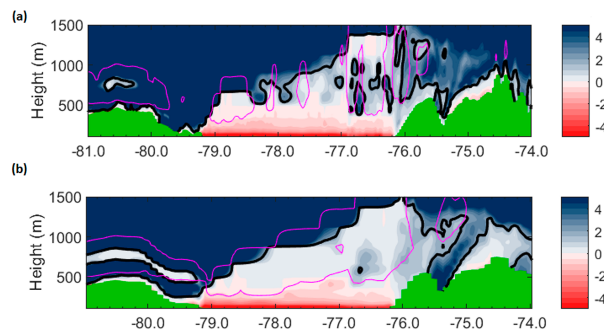


FIG. A1. Comparison of 44°N cross sections of static stability for Lake Ontario at 1200 UTC 8 Jan 2014 using (a) 3-km (WRF domain 3) and (b) 9-km (WRF domain 2) horizontal grid spacing.

circulations that may be better resolved in the 3-km model are likely smoothed out to some degree in Fig. A1. We recognize that convection-permitting grid spacing would likely lead to a superior representation of these layers; that possibility can be explored in future work.

REFERENCES

Agree, E. M., and S. R. Gilbert, 1989: An aircraft investigation of mesoscale convection over Lake Michigan during the 10 January 1984 cold air outbreak. *J. Atmos. Sci.*, **46**, 1877–1897, [https://doi.org/10.1175/1520-0469\(1989\)046<1877:AAIOMC>2.0.CO;2](https://doi.org/10.1175/1520-0469(1989)046<1877:AAIOMC>2.0.CO;2).

Banacos, P. C., and M. L. Ekster, 2010: The association of the elevated mixed layer with significant severe weather events in the northeastern United States. *Wea. Forecasting*, **25**, 1082–1102, <https://doi.org/10.1175/2010WAF2222363.1>.

Bergmaier, P. T., B. Geerts, L. S. Campbell, and W. J. Steenburgh, 2017: The OWLeS IOP2b lake-effect snowstorm: Dynamics of the secondary circulation. *Mon. Wea. Rev.*, **145**, 2437–2459, <https://doi.org/10.1175/MWR-D-16-0462.1>.

Carlson, T. N., and F. H. Ludlam, 1968: Conditions for the occurrence of severe local storms. *Tellus*, **20**, 203–226, <https://doi.org/10.1111/j.2153-3490.1968.tb00364.x>.

—, S. G. Benjamin, G. S. Forbes, and Y.-F. Li, 1983: Elevated mixed layers in the Regional Severe Storm Environment: Conceptual model and case studies. *Mon. Wea. Rev.*, **111**, 1453–1474, [https://doi.org/10.1175/1520-0493\(1983\)111<1453:EMLTR>2.0.CO;2](https://doi.org/10.1175/1520-0493(1983)111<1453:EMLTR>2.0.CO;2).

Chang, S. S., and R. R. Braham Jr., 1991: Observational study of a convective internal boundary layer over Lake Michigan. *J. Atmos. Sci.*, **48**, 2265–2279, [https://doi.org/10.1175/1520-0469\(1991\)048<2265:OISACI>2.0.CO;2](https://doi.org/10.1175/1520-0469(1991)048<2265:OISACI>2.0.CO;2).

Chen, F., and J. Dudhia, 2001: Coupling an advanced land-surface-hydrology model with the Penn State-NCAR MM5 modeling system. Part I: Model implementation and sensitivity. *Mon. Wea. Rev.*, **129**, 569–585, [https://doi.org/10.1175/1520-0493\(2001\)129<0569:CAALSH>2.0.CO;2](https://doi.org/10.1175/1520-0493(2001)129<0569:CAALSH>2.0.CO;2).

Clark, R., 2014: Millersville University Mobile Radiosonde Data, version 1.0. UCAR/NCAR–Earth Observing Laboratory, accessed 30 October 2023, <https://doi.org/10.26023/X8R4-CB1B-VY0X>.

Conrick, R., H. D. Reeves, and S. Zhong, 2015: The dependence of QPF on the choice of boundary-and surface-layer parameterization for a lake-effect snowstorm. *J. Appl. Meteor. Climatol.*, **54**, 1177–1190, <https://doi.org/10.1175/JAMC-D-14-0291.1>.

Cordeira, J. M., N. D. Metz, M. E. Howarth, and T. J. Galarneau, 2017: Multiscale upstream and in situ precursors to the elevated mixed layer and high-impact weather over the Midwest United States. *Wea. Forecasting*, **32**, 905–923, <https://doi.org/10.1175/WAF-D-16-0122.1>.

—, D. T., G. S. Young, S. J. Greybush, S. Saslo, T. D. Sikora, and R. D. Clark, 2018: Predicting the inland penetration of long-lake-axis parallel snowbands. *Wea. Forecasting*, **33**, 1435–1451, <https://doi.org/10.1175/WAF-D-18-0033.1>.

—, S. J. Greybush, G. S. Young, S. Saslo, T. D. Sikora, and R. D. Clark, 2019: Lake-effect snowbands in baroclinic environments. *Wea. Forecasting*, **34**, 1657–1674, <https://doi.org/10.1175/WAF-D-18-0191.1>.

Eure, K. C., P. D. Mykolajtchuk, Y. Zhang, D. J. Stensrud, F. Zhang, S. J. Greybush, and M. R. Kumjian, 2023: Simultaneous assimilation of planetary boundary layer observations from radar and all-sky satellite observations to improve forecasts of convection initiation. *Mon. Wea. Rev.*, **151**, 795–813, <https://doi.org/10.1175/MWR-D-22-0188.1>.

Garrett, A. J., 1981: Comparison of observed mixed-layer depths to model estimates using observed temperatures and winds, and MOS forecasts. *J. Appl. Meteor.*, **20**, 1277–1283, [https://doi.org/10.1175/1520-0450\(1981\)020<1277:COOMLD>2.0.CO;2](https://doi.org/10.1175/1520-0450(1981)020<1277:COOMLD>2.0.CO;2).

Grell, G. A., and D. Dévényi, 2002: A generalized approach to parameterizing convection combining ensemble and data assimilation techniques. *Geophys. Res. Lett.*, **29**, 1693, <https://doi.org/10.1029/2002GL015311>.

Greybush, S. J., and G. S. Young, 2023: The lake-effect snow ensemble reanalysis version 1.0 dataset. Penn State Data Commons, accessed 3 November 2023, <https://doi.org/10.26208/Q845-PN39>.

Hjelmfelt, M. R., 1990: Numerical study of the influence of environmental conditions on lake-effect snowstorms over Lake Michigan. *Mon. Wea. Rev.*, **118**, 138–150, [https://doi.org/10.1175/1520-0493\(1990\)118<0138:NSOTIO>2.0.CO;2](https://doi.org/10.1175/1520-0493(1990)118<0138:NSOTIO>2.0.CO;2).

—, and R. R. Braham Jr., 1983: Numerical simulation of the airflow over Lake Michigan for a major lake-effect snow event. *Mon. Wea. Rev.*, **111**, 205–219, [https://doi.org/10.1175/1520-0493\(1983\)111<0205:NSOTAO>2.0.CO;2](https://doi.org/10.1175/1520-0493(1983)111<0205:NSOTAO>2.0.CO;2).

Janjić, Z. I., 1994: The step-mountain Eta coordinate model: Further developments of the convection, viscous sublayer, and turbulence closure schemes. *Mon. Wea. Rev.*, **122**, 927–945, [https://doi.org/10.1175/1520-0493\(1994\)122<0927:TSMECM>2.0.CO;2](https://doi.org/10.1175/1520-0493(1994)122<0927:TSMECM>2.0.CO;2).

—, 1996: The surface layer in the NCEP Eta Model. *Preprints, 11th Conf. on Numerical Weather Prediction*, Norfolk, VA, Amer. Meteor. Soc., 354–355.

—, 2002: Nonsingular implementation of the Mellor–Yamada level 2.5 scheme in the NCEP Meso model. NCEP Office Note 437, National Centers for Environmental Prediction, 61 pp.

Kristovich, D., 2014: University of Illinois Mobile Radiosonde Data, version 1.0. UCAR/NCAR–Earth Observing Laboratory, accessed 30 October 2023, <https://doi.org/10.26023/DM6C-VWE6-7Q07>.

—, and Coauthors, 2000: The Lake-Induced Convection Experiment and the Snowband Dynamics Project. *Bull. Amer. Meteor. Soc.*, **81**, 519–542, [https://doi.org/10.1175/1520-0477\(2000\)081<0519:TLCEAT>2.3.CO;2](https://doi.org/10.1175/1520-0477(2000)081<0519:TLCEAT>2.3.CO;2).

—, and Coauthors, 2017: The Ontario Winter Lake-Effect Systems Field Campaign: Scientific and educational adventures to further our knowledge and prediction of lake-effect

storms. *Bull. Amer. Meteor. Soc.*, **98**, 315–332, <https://doi.org/10.1175/BAMS-D-15-00034.1>.

Laird, N., and N. Metz, 2014: Hobart and William Smith Colleges Mobile Radiosonde Data, version 1.0. UCAR/NCAR–Earth Observing Laboratory, accessed 30 October 2023, <https://doi.org/10.26023/9BXB-WWGD-2A0B>.

—, J. E. Walsh, and D. A. R. Kristovich, 2003: Model simulations examining the relationship of lake-effect morphology to lake shape, wind direction, and wind speed. *Mon. Wea. Rev.*, **131**, 2102–2111, [https://doi.org/10.1175/1520-0493\(2003\)131<2102:MSETRO>2.0.CO;2](https://doi.org/10.1175/1520-0493(2003)131<2102:MSETRO>2.0.CO;2).

Lavoie, R. L., 1972: A mesoscale numerical model of lake effect snowstorms. *J. Atmos. Sci.*, **29**, 1025–1040, [https://doi.org/10.1175/1520-0469\(1972\)029<1025:AMNMOL>2.0.CO;2](https://doi.org/10.1175/1520-0469(1972)029<1025:AMNMOL>2.0.CO;2).

Lee, J. A., L. J. Peltier, S. E. Haupt, J. C. Wyngaard, D. R. Stauffer, and A. Deng, 2009: Improving SCIPUFF dispersion forecasts with NWP ensembles. *J. Appl. Meteor. Climatol.*, **48**, 2305–2319, <https://doi.org/10.1175/2009JAMC2171.1>.

Lenschow, D. H., 1973: Two examples of planetary boundary layer modification over the Great Lakes. *J. Atmos. Sci.*, **30**, 568–581, [https://doi.org/10.1175/1520-0469\(1973\)030<0568:TEOPBL>2.0.CO;2](https://doi.org/10.1175/1520-0469(1973)030<0568:TEOPBL>2.0.CO;2).

Minder, J. R., W. M. Bartolini, C. Spence, N. R. Hedstrom, P. D. Blanken, and J. D. Lenters, 2020: Characterizing and constraining uncertainty associated with surface and boundary layer turbulent fluxes in simulations of lake-effect snowfall. *Wea. Forecasting*, **35**, 467–488, <https://doi.org/10.1175/WAF-D-19-0153.1>.

Nielsen-Gammon, J. W., and Coauthors, 2008: Multisensor estimation of mixing heights over a coastal city. *J. Appl. Meteor. Climatol.*, **47**, 27–43, <https://doi.org/10.1175/2007JAMC1503.1>.

Niziol, T. A., 1987: Operational forecasting of lake effect snowfall in western and central New York. *Wea. Forecasting*, **2**, 310–321, [https://doi.org/10.1175/1520-0434\(1987\)002<0310:OFOLES>2.0.CO;2](https://doi.org/10.1175/1520-0434(1987)002<0310:OFOLES>2.0.CO;2).

Reinking, R. F., and Coauthors, 1993: The Lake Ontario Winter Storms (LOWs) project. *Bull. Amer. Meteor. Soc.*, **74**, 1828–1850, <https://doi.org/10.1175/1520-0477-74-10-1828>.

Ribeiro, B. Z., and L. F. Bosart, 2018: Elevated mixed layers and associated severe thunderstorm environments in South and North America. *Mon. Wea. Rev.*, **146**, 3–28, <https://doi.org/10.1175/MWR-D-17-0121.1>.

Saslo, S., and S. J. Greybush, 2017: Prediction of lake-effect snow using convection-allowing ensemble forecasts and regional data assimilation. *Wea. Forecasting*, **32**, 1727–1744, <https://doi.org/10.1175/WAF-D-16-0206.1>.

Schroeder, J. J., D. A. R. Kristovich, and M. R. Hjelmfelt, 2006: Boundary layer and microphysical influences of natural cloud seeding on a lake-effect snowstorm. *Mon. Wea. Rev.*, **134**, 1842–1858, <https://doi.org/10.1175/MWR3151.1>.

Seibert, J. J., S. J. Greybush, J. Li, Z. Zhang, and F. Zhang, 2022: Applications of the geometry-sensitive ensemble mean for lake-effect snowbands and other weather phenomena. *Mon. Wea. Rev.*, **150**, 409–429, <https://doi.org/10.1175/MWR-D-21-0212.1>.

Sikora, T. D., R. D. Clark, D. T. Eipper, S. J. Greybush, M. L. Jurowicz Sr., D. A. R. Kristovich, and G. S. Young, 2015: Origin and frequency of near-surface statically stable layers and elevated weak-static stability layers during the Ontario Winter Lake-Effect Systems (OWLeS) project. *Twentieth Conf. on Air-Sea Interaction*, Madison, WI, Amer. Meteor. Soc., 12.2, <https://ams.confex.com/ams/95Annual/webprogram/Paper263079.html>.

Skamarock, W. C., and Coauthors, 2008: A description of the Advanced Research WRF version 3. NCAR Tech. Note NCAR/TN-475+STR, 113 pp., <https://doi.org/10.5065/D68S4MVH>.

Sousounis, P. J., and G. E. Mann, 2000: Lake-aggregate mesoscale disturbances. Part V: Impacts on lake-effect precipitation. *Mon. Wea. Rev.*, **128**, 728–745, [https://doi.org/10.1175/1520-0493\(2000\)128<0728:LAMDPV>2.0.CO;2](https://doi.org/10.1175/1520-0493(2000)128<0728:LAMDPV>2.0.CO;2).

Steenburgh, W. J., and L. S. Campbell, 2017: The OWLeS IOP2b lake-effect snowstorm: Shoreline geometry and the mesoscale forcing of precipitation. *Mon. Wea. Rev.*, **145**, 2421–2436, <https://doi.org/10.1175/MWR-D-16-0460.1>.

—, —, and P. Veals, 2014: University of Utah North Redfield Radiosonde Data, version 1.0. UCAR/NCAR–Earth Observing Laboratory, accessed 30 October 2023, <https://doi.org/10.26023/RH2Y-8E1R-G905>.

Steiger, S., 2014: SUNY-Oswego Mobile Radiosonde Data, version 1.0. UCAR/NCAR–Earth Observing Laboratory, accessed 30 October 2023, <https://doi.org/10.26023/1RXB-B0BX-D00>.

—, and Coauthors, 2013: Circulations, bounded weak echo regions, and horizontal vortices observed within long-lake-axis-parallel-lake-effect storms by the Doppler on Wheels. *Mon. Wea. Rev.*, **141**, 2821–2840, <https://doi.org/10.1175/MWR-D-12-002261>.

Stull, R. B., 1988: *An Introduction to Boundary Layer Meteorology*. Springer, 670 pp.

Thompson, G., P. R. Field, R. M. Rasmussen, and W. D. Hall, 2008: Explicit forecasts of winter precipitation using an improved bulk microphysics scheme. Part II: Implementation of a new snow parameterization. *Mon. Wea. Rev.*, **136**, 5095–5115, <https://doi.org/10.1175/2008MWR2387.1>.

Tripoli, G. J., 2005: Numerical study of the 10 January 1998 lake-effect bands observed during Lake-ICE. *J. Atmos. Sci.*, **62**, 3232–3249, <https://doi.org/10.1175/JAS3462.1>.

Weng, Y., and F. Zhang, 2012: Assimilating airborne Doppler radar observations with an ensemble Kalman filter for convection-permitting hurricane initialization and prediction: Katrina (2005). *Mon. Wea. Rev.*, **140**, 841–859, <https://doi.org/10.1175/2011MWR3602.1>.

Whitaker, J. S., and T. M. Hamill, 2002: Ensemble data assimilation without perturbed observations. *Mon. Wea. Rev.*, **130**, 1913–1924, [https://doi.org/10.1175/1520-0493\(2002\)130<1913:EDAWPO>2.0.CO;2](https://doi.org/10.1175/1520-0493(2002)130<1913:EDAWPO>2.0.CO;2).

Young, G. S., D. A. R. Kristovich, M. R. Hjelmfelt, and R. C. Foster, 2002: Rolls, streets, waves, and more: A review of quasi-two-dimensional structures in the atmospheric boundary layer. *Bull. Amer. Meteor. Soc.*, **83**, 997–1001.

Zhang, F., Z. Meng, and A. Aksoy, 2006: Tests of an ensemble Kalman filter for mesoscale and regional-scale data assimilation. Part I: Perfect model experiments. *Mon. Wea. Rev.*, **134**, 722–736, <https://doi.org/10.1175/MWR3101.1>.